Published in final edited form as:
Cancer Cell. 2013 December 9; 24(6): 751–765. doi:10.1016/j.ccr.2013.10.013.

Transformation of the Fallopian Tube Secretory Epithelium Leads to High-grade Serous Ovarian Cancer in *Brca;Tp53;Pten* Models

Ruth Perets[1,#,¶], **Gregory A. Wyant**[2,#], **Katherine W. Muto**[2], **Jonathan G. Bijron**[3], **Barish B. Poole**[2], **Kenneth T. Chin**[2], **Jin Yun H. Chen**[2], **Anders W. Ohman**[2], **Corey D. Stepule**[2], **Soongu Kwak**[1], **Alison M. Karst**[1], **Michelle S. Hirsch**[3], **Sunita R. Setlur**[2], **Christopher P. Crum**[3], **Daniela M. Dinulescu**[2,3,*], and **Ronny Drapkin**[1,3,*]

[1]Department of Medical Oncology, Center for Molecular Oncologic Pathology, Dana-Farber Cancer Institute, Harvard Medical School, Boston, MA 02215

[2]Eugene Braunwald Research Center, Department of Pathology, Harvard Medical School, Boston, MA 02115

[3]Department of Pathology, Division of Women's and Perinatal Pathology, Brigham & Women's Hospital, Harvard Medical School, Boston, MA 02115

Summary

High-grade serous ovarian carcinoma presents significant clinical and therapeutic challenges. Although the traditional model of carcinogenesis has focused on the ovary as a tumor initiation site, recent studies suggest that there may be additional sites of origin outside the ovary, namely the secretory cells of the fallopian tube. Our study demonstrates that high-grade serous tumors can originate in fallopian tubal secretory epithelial cells and also establishes serous tubal intraepithelial carcinoma as the precursor lesion to high-grade serous ovarian and peritoneal carcinomas in animal models targeting the *Brca*, *Tp53*, and *Pten* genes. These findings offer an

[*]Corresponding senior authors: Daniela M. Dinulescu, ddinulescu@rics.bwh.harvard.edu, Phone: 617-732-5318. Ronny Drapkin, ronny_drapkin@dfci.harvard.edu, Phone: 617-632-4380.
[#]Indicates equal contribution
[¶]Current address: Oncology Division, Rambam Health Care Campus, Haifa, Israel 31096

Supplemental Information
Supplemental Data includes 6 figures, 6 tables, Supplemental Experimental Procedures, and Supplemental References.

Accession number
The array CGH data files have been deposited in the Gene Expression Omnibus repository (http://www.ncbi.nlm.nih.gov/geo/). The accession number is GSE49827.

Author Contributions
R.P., D.M.D., and R.D. provided the concept design for these studies. R.P., G.A.W., K.W.M., D.M.D., and R.D. devised and designed the experiments. R.P. generated and characterized the *Pax8-Cre* deletor mouse. G.A.W., K.W.M., B.B.P., K.T.C., A.W.O., and C.D.S. developed and characterized the *Brca* FT animal models. R.P., G.A.W., and S.K. performed Western Blot analysis. J.G.B. performed immunohistochemical analysis. J.G.B., M.S.H., and C.P.C. provided expert pathological analysis, clinical insight, and pertinent suggestions. A.M.K. and R.D. generated FTSEC lines. J.H.C. and S.R.S. performed genomic experiments and bioinformatics analysis. R.P., G.A.W., K.W.M., A.W.O, S.R.S., D.M.D., and R.D. analyzed the data and wrote the manuscript.

Competing Interests Statement
The authors declare that they have no competing financial interests.

avenue to address clinically important questions that are critical for cancer prevention and early detection in women carrying *BRCA1* and *BRCA2* mutations.

Introduction

Epithelial ovarian cancer is the most lethal gynecologic malignancy in the United States with an annual mortality rate of 15,000 (Siegel et al., 2012). High-grade serous ovarian carcinoma (HGSC), the most common and aggressive subtype, has the highest mortality rate, with a 5-year survival rate of only 30% (Vaughan et al., 2011). This is due to the fact that the vast majority of cases are not detected until late-stage, ultimately thwarting attempts to define the cell-of-origin and pathogenesis of this disease.

Although research has traditionally focused on the hypothesis that HGSC arises from the ovarian surface epithelium (OSE) or ovarian inclusion cysts, recent studies suggest that additional sites of origin exist and a substantial proportion of cases may arise from precursor lesions located in the fallopian tubal epithelium (FTE). The latter hypothesis is based on the detection of early lesions, namely serous tubal intraepithelial carcinomas (STIC), found in the fallopian tubes (FT) of both women at high-risk for developing serous carcinomas as well as patients with disseminated HGSCs (Kindelberger et al., 2007; Lee et al., 2007; Leeper et al., 2002; Levanon et al., 2008; Medeiros et al., 2006; Przybycin et al., 2010). Recent studies of ovarian and tubal tissue samples from high-risk *BRCA1/2* mutation carriers who underwent prophylactic salpingo-oophorectomy procedures to reduce their cancer risk revealed early cancer lesions in ~5–15% of cases, with 60–100% of lesions found in the FT fimbria (Leeper et al., 2002; Medeiros et al., 2006). In addition, STIC lesions, which are defined as *in situ* cancers with *TP53* mutations and increased proliferative capacity, are observed in at least 60% of women with HGSC of the ovary and/or peritoneum (Kindelberger et al., 2007; Przybycin et al., 2010) and similar *in situ* lesions are not observed in the OSE (Folkins et al., 2008). Such early lesions exhibit shortened telomeres, a notable hallmark of early molecular carcinogenesis (Kuhn et al., 2011) (Chene et al., 2013). Clinical observations support the hypothesis that STICs can originate from secretory epithelial cells of the fallopian tube and progress to HGSC by rapidly disseminating to involve ovarian and peritoneal surfaces. This hypothesis is further supported by the shared morphologic and immunophenotypic features of STICs and HGSCs. In addition, injection of transformed primary human FT secretory epithelial cells (FTSECs) into the peritoneum of nude mice induces tumors that grossly, histologically, immunophenotypically, and genomically resemble human HGSCs (Karst et al., 2011a) (Jazaeri et al., 2011). However, these associations are largely circumstantial and necessitate experimental proof in order to confirm the role of FTSECs and STICs in serous carcinogenesis. The vast implications of unequivocally establishing a potential cell of origin in HGSC for both cancer prevention and early tumor detection prompted us to develop genetically engineered animal models that mimic human HGSC pathogenesis.

Genetically engineered mouse models for the endometrioid subtype of ovarian cancer have been successfully exploited to resolve the site of origin and pathogenesis for this particular subtype (Dinulescu et al., 2005; Wu et al., 2007; Wu et al., 2013). In contrast, an effective *de novo* mouse model for HGSC has proven elusive, likely because previous models were designed based on traditional views of ovarian cancer pathogenesis, namely strictly ovarian origin. Previous work has utilized conditional expression of oncogenes (for instance, *Kras*) or conditional deletion of relevant tumor suppressors (such as *Brca1/2*, *Tp53*, *Rb*, and *Pten*); while these markers are well defined in the literature, all have targeted the OSE (Clark-Knowles et al., 2007; Clark-Knowles et al., 2009; Flesken-Nikitin et al., 2003; Mullany et al., 2011; Quinn et al., 2009; Szabova et al., 2012). Subsequently some tumors have failed to recapitulate the histology and markers of the human disease (Clark-Knowles et al., 2007;

Clark-Knowles et al., 2009; Mullany et al., 2011; Quinn et al., 2009). Another study utilized an activating *Pik3ca* mutation coupled with *Pten* loss to drive ovarian serous carcinoma from the OSE, but this also resulted in granulosa cell and luteoma tumors and did not recapitulate early precursor lesions (Kinross et al., 2012). A recent study targeted deletion of *Pten* and *Dicer*, the ribonuclease essential for the conversion of pre-miRNAs into mature miRNAs, using the anti-Mullerian hormone receptor type 2 promoter to drive Cre expression. While these animals developed tumors in the FT, they failed to recapitulate the early events of human disease pathogenesis, namely FTSEC transformation and STIC lesions (Kim et al., 2012). Collectively, these studies all suggest that the origin of HGSC is still unknown and may arise from multiple sources. However, developing a genetically engineered mouse model of HGSC, which accurately recapitulates the early alterations and disease progression seen in patients and high-risk women, is key to improving early cancer diagnosis and is an important goal of our study. Such a model can confirm the transformation continuum from STIC to HGSC and mimic the molecular alterations underlying this process.

Results

PAX8 is a Marker of the Fallopian Tube Secretory Cell but Not of the Ovarian Surface Epithelium

We have specifically targeted the FTSEC by driving expression of the Cre recombinase from a *Pax8* promoter. PAX8 is a transcription factor that is essential for the development of the female genital tract, including the FTs but not the ovaries (Mittag et al., 2007). In the FTE, PAX8 is a marker of the secretory cell lineage, not the ciliated cell population (Figure 1A, B). Consistent with its role as a lineage marker (Bowen et al., 2007; Cheung et al., 2011), PAX8 expression is retained in the FT cells during the process of secretory cell malignant transformation, both in STIC lesions (Figure 1A, B) and in the vast majority of HGSCs (Figure 1C) (Laury et al., 2010; Laury et al., 2011; Tacha et al., 2011). In mouse FTE, PAX8 shows a similar pattern of expression in FTSECs and is not present in acetylated tubulin-positive ciliated cells (Figures 1D–F). Importantly, PAX8 is absent in mouse and human OSE (Figure 1D) (Bowen et al., 2007). This distinct PAX8 expression pattern was confirmed by Western Blot analysis, which showed strong PAX8 expression in human FTSEC lines and no expression in human ovarian surface epithelial (HOSE) cell lines (Figure 1G).

PAX8 can drive Cre-recombinase in the Fallopian Tube Secretory Cell

In order to express Cre recombinase from the mouse FTSEC, we crossed mice expressing the reverse tetracycline-controlled transactivator (*rtTA*) under the control of the *Pax8* promoter (*Pax8-rtTA*) with mice expressing Cre recombinase in a tetracycline dependent manner (*TetO-Cre*) (Perl et al., 2002; Traykova-Brauch et al., 2008). The combination of both transgenes, which we termed *Pax8-Cre*, was used as a tissue specific driver for all genetic alterations described hereafter (Figure S1A). In order to determine the tissue specificity of the recombination event, *Pax8-Cre* mice were crossed with *Gt(ROSA)26Sor*^{tm1sor} mice expressing the *loxP-Stop-loxP LacZ* transgene (Figure S1A) (Soriano, 1999). Following administration of doxycycline (Dox, 0.2mg/ml in drinking water *ad libitum*) for 14 days to activate Cre-mediated recombination, organs were harvested and subjected to β-galactosidase staining. Gross anatomic inspection showed that the FT exhibited a very strong LacZ staining pattern; some staining was observed in the uterus and, importantly, the ovary was completely negative for LacZ (Figure 1H, I). Histologically, as expected from the mosaic pattern of Pax8-positive secretory and Pax8-negative ciliated cells, the FTE exhibited a mosaic pattern of LacZ staining (Figure 1J). Most importantly, microscopic evaluation of the OSE did not exhibit any LacZ staining (Figure S1B, C)

thereby confirming that HGSC in this model cannot arise from the OSE. As expected, the FTE of *Pax8-rtTA;LSL-LacZ* mice, without *TetO-Cre* (negative control) showed no LacZ staining (Figure S1D, E). In addition, endometrial and renal tubular epithelium expressed LacZ (Figure S1F, G and Traykova-Brauch et al., 2008), while the liver showed focal LacZ staining in scattered hepatocytes (Traykova-Brauch et al., 2008). As previously shown, the thyroid, another PAX8-expressing organ, does not express *rtTA* in this *Pax8-rtTA* mouse strain (Traykova-Brauch et al., 2008) and was negative for LacZ expression (Figure S1H, I). No other organs displayed LacZ staining.

Murine cohorts were generated harboring *Pax8-Cre* driven inactivation of different combinations of the *Brca* (*Brca1* or *Brca2*), *Tp53* (loss of function and/or dominant negative inactivating *R270H* mutation), and *Pten* genes, which are commonly altered in ovarian cancer patients (Figure 2A–D) (TCGA, 2011). Heterozygous and homozygous *Brca1* (and *Brca2*) mutants (mut), unless otherwise indicated, will collectively be designated $Brca1^{mut}$ *(*$Brca2^{mut}$*)* as they yielded similar tumor phenotypes. Similarly, $Tp53^{-/-}$ gave similar results as $Tp53^{R270H/-}$ and therefore are collectively designated $Tp53^{mut}$. The Kaplan-Meier curves of the 5 *Pax8-rtTA;TetO-Cre* murine cohorts, $Brca1^{-/-};Tp53^{mut};Pten^{-/-}$, $Brca1^{+/-};Tp53^{mut};Pten^{-/-}$, $Brca2^{-/-};Tp53^{mut};Pten^{-/-}$, $Brca2^{+/-};Tp53^{mut};Pten^{-/-}$, and $Tp53^{-/-};Pten^{-/-}$ mice are shown for comparison in Figure 2C. Interestingly, we noticed a statistically significant increase in disease latency in the $Tp53^{-/-};Pten^{-/-}$ cohort in comparison to either $Brca1^{mut};Tp53^{mut};Pten^{-/-}$ or $Brca2^{mut};Tp53^{mut};Pten^{-/-}$ mice ($p < 0.01$, Figure 2C). Furthermore, the survival of $Brca2^{-/-}$ mice was significantly lower when compared to $Brca2^{+/-}$ mice ($p < 0.05$, Figure 2C). Otherwise, the heterozygous and homozygous *Brca1* and *Brca2* animals yielded similar phenotypic results. Evidence of *Brca2*, *Tp53*, and *Pten* recombination in our animal models is shown in Figure 2D while the efficiency of recombination events at the 3 genetic loci is displayed in Figure 2E. Tumors that show incomplete recombination likely reflect the presence of stromal and/or ciliated epithelial cells that are not targeted. In patients, *BRCA1* and *BRCA2* are known to be associated with hereditary breast and ovarian cancer. In the recently published TCGA data *BRCA*1 and *BRCA*2 show germline mutations in 9% and 8% of HGSC cases, respectively, and somatic mutations in an additional 3% of cases (TCGA, 2011). In addition, *BRCA1* and *BRCA2* germline mutation frequency is as high as 17% of cases in a large series of Australian HGSC patients (Alsop et al., 2012). In addition, *TP53* is mutated in the vast majority (96%) of human HGSC cases. Furthermore, according to TCGA data, while homozygous loss of *PTEN* is seen in only 7% of ovarian cancer cases, the PI3K/PTEN pathway is aberrant in 74.4% of HGSC cases (Figure S2). More specifically, TCGA analysis shows combined alterations, including mutations, single and/or double copy deletions of *BRCA1*, *TP53*, and *PTEN* to be prevalent in 31% of cases, with homozygous loss of *PTEN* being present in 8% of cases harboring *BRCA1;TP53* alterations (Table S1). A similar TCGA analysis for *BRCA2* reveals co-existing alterations, including mutations, single and/or double copy deletions of *BRCA2*, *TP53*, and *PTEN* in 25% of cases, with homozygous *PTEN* loss being present in 7% of *BRCA2;TP53* altered cases (Table S2). Therefore, alterations in *BRCA1/2*, *TP53*, and *PTEN* genes serve as a relevant model for human FT transformation and development of HGSC in patients.

Pax8-driven Deletions of *Brca*, *Tp53*, and *Pten* Lead to Development of HGSCs Arising From FTSECs

Cre-mediated recombination in both $Brca1^{mut};Tp53^{mut};Pten^{-/-}$ and $Brca2^{mut};Tp53^{mut};Pten^{-/-}$ mice led to development of HGSCs following Dox administration. In contrast to a normal murine FT (Figure 3A), Dox-activated FTs underwent transformation marked by secretory cell proliferation, loss of polarity, cellular atypia, and serous histology, all consistent with STIC (Figure 3B–D and data not shown). In

all invasive carcinomas that metastasized to the ovary and peritoneum, the histology was characteristic of HGSC (Figure 3E–H and data not shown). HGSC tumors metastasized to the ovary in 7/16 *Brca1^{mut};Tp53^{mut};Pten$^{-/-}$* and 12/15 *Brca2^{mut};Tp53^{mut};Pten$^{-/-}$* mice (Figure 3F and data not shown). In 5/16 *Brca1^{mut};Tp53^{mut};Pten$^{-/-}$* and 3/15 *Brca2^{mut};Tp53 ^{mut};Pten$^{-/-}$* mice, the tumor metastasized to the liver (Figure 3G and data not shown) and in 9/16 *Brca1^{mut};Tp53^{mut};Pten$^{-/-}$* and 10/15 *Brca2^{mut};Tp53^{mut};Pten$^{-/-}$* mice, the tumor metastasized to the peritoneal cavity (Figure 3E, H and data not shown). Although the omentum was typically involved, peritoneal involvement was generally widespread and we did not discern between the different organs involved or the omentum. These findings are consistent with the pattern of HGSC spread in humans. Frequent ovarian metastases are of special interest since HGSC is commonly diagnosed in the ovary. Immunohistochemical analysis of murine pre-invasive and invasive lesions demonstrated a high degree of concordance between human and mouse tumor markers (Figure 3I). Thus, PAX8 serves as the hallmark for human HGSC diagnosis. In line with our *Pax8*-driven model, murine pre-invasive lesions and invasive tumors were PAX8 positive, similar to human counterparts (Figure 3I). As expected, all murine tumors with dominant negative *Tp53 R270H* mutations showed accumulation of nuclear TP53 immunoreactivity (Figure 3I); in addition, an increased Ki-67 proliferative index was seen in STICs and metastatic lesions (Figure 3I). Thus, the immunohistochemical profiles of murine tumors mimic those of human STICs and HGSC tumors and confirm our targeting strategy. Furthermore, in addition to being positive for PAX8 and Ki-67, murine STIC lesions showed immunoreactivity for Stathmin-1 (STMN1) (Figure 4A–D) in contrast to normal FTE (located adjacent to the STIC, left side of the image, in Figure 4C, D). STMN1 is a marker for early human serous carcinoma that is significantly increased upon progression to STIC and invasive carcinoma in patients (Karst et al., 2011b). As expected, tumors were positive for epithelial markers, including Pan-Keratin and CK8 (Figure 5A). In addition, PAX8-immunoreactive tumors and metastases were also positive for either PAX2 (Figure 5B) or WT-1 (Figure 5C), two markers that are expressed by human HGSCs. As noted earlier, the endometrium expresses *Pax8* and this expression was confirmed with LacZ staining (Figure S1F–G). Because *PTEN* is the most common genetic alteration observed in endometrial neoplasms (Mutter et al., 2000), we closely examined the endometrium in all cohorts of mice. All mice had various degrees of endometrial changes, which recapitulated human endometrial hyperplasia, dysplasia, or carcinoma (Figure S3A). Interestingly, intrauterine endometrial lesions were negative for PAX2 and WT1 markers (Figure S3B, C), whereas the STICs and metastatic HGSC tumors (described above) retained PAX2 expression (Figure S3B) or WT1 expression (Figure S3C), strongly suggesting that the metastatic lesions arose from the FT and not the endometrium.

In order to study the contribution of *Brca* and *Pten* genetic alterations to the pathogenesis of HGSC tumors, we generated control cohorts of *Tp53$^{-/-}$;Pten$^{-/-}$* mice without *Brca* alterations and *Brca2$^{-/-}$;Tp53^{mut}* mice without *Pten* alterations, respectively. Interestingly, the *Tp53$^{-/-}$;Pten$^{-/-}$* mice did not progress past the pre-invasive stage of the disease. Four of six *Tp53$^{-/-}$;Pten$^{-/-}$* mice had tubal transformation and developed STICs at the time of sacrifice (19–38 weeks), but none showed invasive tumors, suggesting that *Brca1* or *Brca2* gene alterations are necessary for the progression of ovarian and peritoneal HGSCs (Figure 2B, C). Although the *Tp53$^{-/-}$;Pten$^{-/-}$* cohort did not develop invasive HGSC, 4/6 mice had to be sacrificed according to veterinary recommendation because of palpable uterine tumors or a visible reduction in body condition, scruffy appearance, and hair loss (at 24 and 38 weeks, respectively), which required euthanasia. Histopathological analysis of the *Tp53$^{-/-}$;Pten$^{-/-}$* mice with uterine tumors showed locally enlarged endometrial tumors but no metastases were detected. The remaining *Tp53$^{-/-}$;Pten$^{-/-}$* mice had to be euthanized due to unrelated conditions (i.e., 1/6 mice developed malocclusion and 1/6 developed a large skin abrasion). Furthermore, in *Brca2$^{-/-}$;Tp53^{mut}* mice, in which *Pten* is wild-type, the

disease latency was much longer (30–43 weeks) and tumorigenesis was inefficient (only 3/11 mice developed peritoneal metastases), suggesting that additional genes are needed to cooperate with *Brca* and *Tp53* deletion or mutation to induce tumor initiation and progression. Interestingly, STICs were difficult to detect in the $Brca2^{-/-};Tp53^{mut}$ mice because invasive disease was widely present at the time that the animals were sacrificed, a not uncommon phenomenon in human HGSC. This in part can explain why STIC lesions are not identified in 100% of HGSCs. More importantly, these results suggest that loss of *Pten* or activation of the PTEN/PI3K pathway is necessary for efficient tumor development and STIC formation in the murine oviduct. Similarly, a recent patient study indicated that PTEN expression was markedly reduced or absent in one-third of human STICs (Roh et al., 2010).

Salpingectomies, Oophorectomies, and Hysterectomies in Pax8-driven BRCA Models Support a Tubal Origin for HGSC

In order to further rule out the endometrial origin of HGSC metastases in our mice, we performed hysterectomies and salpingectomies in $Brca1^{mut};Tp53^{mut};Pten^{-/-}$ and $Brca2^{mut};Tp53^{mut};Pten^{-/-}$ murine cohorts. Uterus removal by hysterectomy resulted in STICs and tubal transformation in all mice, ovarian HGSC invasion in 3/6 mice and peritoneal HGSC metastases in 5/6 animals at 9–12 weeks post-Cre induction (Figure 6A–F, Figure S4A). Immunohistochemical and pathological analysis of STICs and ovarian/peritoneal tumor metastases in the hysterectomy cohort was consistent with HGSC profiles (Figure 6F). Invasive tumors were positive for human epithelial and HGSC markers, such as CK8, PAX8, WT1, and TP53 (Figure 6F). In contrast, FT removal by salpingectomy resulted in absence of HGSC in all mice and no metastases (Figure S4A–C). Interestingly, removal of the ovary resulted in generation of STICs and tubal transformation in all mice but reduced peritoneal metastasis, suggesting that the ovary induces a permissive environment for advanced disease, possibly through the role of ovarian hormones or through a mechanism that promotes metastatic spread (Figure S4A, D). It is possible that the ovaries are preferential sites of early metastatic disease and facilitate growth or they produce hormones that encourage peritoneal spread. However, since we sacrificed the oophorectomized cohort within a similar timeline as our intact ovary animals, we cannot rule out that the development of metastatic disease in these mice may necessitate longer times than the timeline we studied.

PAX8-driven tumors show human HGSC biomarkers and genomically correlate with human TCGA data

Serum was collected and tested for the presence of CA-125, the best characterized serum biomarker for human HGSC (Bast, 2003). All mice showed significantly higher CA-125 levels than control mice (Figure 7A). To prove that the elevated CA-125 biomarker detected in the bloodstream is originating from HGSCs, CA-125 was further assessed in tumor samples using Western Blot analysis. As expected, tumor samples showed increased levels of CA-125 in comparison to control murine FTs (Figure 7B). In addition, Western analysis of tumor samples showed increased γH2A.X expression in murine HGSCs in comparison to normal FT, supporting our previous report that the transformation process of FTSEC to HGSC is characterized by the acquisition of abundant DNA damage (Figure 7B) (Levanon et al., 2008).

We further performed a genomic copy number analysis of HGSC tumors isolated from $Brca2^{-/-};Tp53^{mut};Pten^{-/-}$ mice using array comparative genomic hybridization (aCGH) studies (Figure 7C). The analyzed tumors showed the presence of a large number of genomic copy number alterations, including recurrent alterations (Figure 7C), similar to the abundance of copy number alterations recently reported in human HGSCs (TCGA, 2011). In order to compare the regions of copy number alterations in the mouse HGSC model with

those seen in patients, we performed orthology mapping and correlated the syntenic regions with recurrent alterations reported by The Cancer Genome Atlas (TCGA), using the cbio portal (www.cbioportal.org; Cerami et al., 2012) (TCGA, 2011). Interestingly, array CGH analysis revealed several genomic alterations in the mouse models that correlated with significant copy number alterations in the human TCGA dataset (Table 1, Tables S3–S5). This overlap was found to be statistically significant ($p < 0.001$) by random permutation analysis (Figure S5). This analysis identified multiple syntenic regions that overlapped with the top 20 significant recurrent alterations from the TCGA dataset (Table 1, Table S6). *C-MYC* and *KRAS*, among the top recurrent amplifications in the TCGA dataset, were also amplified in our murine models with *Kras* showing recurrent amplifications in two of the three mouse models. We also found many alterations in genes that mapped to pathways reported by TCGA, namely DNA Damage (*ATM, RAD17*), DNA repair and HR-mediated repair (*ATM, TEX15, PALB2, FANCC, TERT*), FOXM1 cell cycle pathway (*FOXM1, SKP2*), NOTCH pathway (*KRT1, PPARG, NUMB, SEL1*), RAS/MAPK signaling (*KRAS, MAPK15*), RB pathway (*E2F7*), and PI3K/MYC (*PIK3R1, FOXO3, RICTOR, c-MYC*) signaling, respectively (Table 1, Figure S6, Tables S3–S6) (TCGA, 2011). Other significant recurrently TCGA altered genes that were also detected in the mouse tumors included tumor suppressor genes (*APC2, WWOX, ANKRD11, INPP4B*), as well as *A2M, POLK*, and *CDK7* (Table 1, Tables S5–S6). Interestingly, large regions of aneuploidy were seen to harbor genes that are syntenic to cancer related genes in patients, such as *APC2, CDH1, PIK3R1, MAPK15, and INPP4B*. Importantly, *INPP4B* is emerging as a new tumor suppressor gene in both ovarian and breast cancers. Loss of heterozygosity at *4q31.21*, the chromosomal region containing the *INPP4B* gene occurs in up to 60% of *BRCA1* mutant and triple-negative/basal-like breast carcinomas and 39.8% of ovarian cancer cases (Gewinner et al., 2009; Bertucci et al., 2013). Furthermore, reduced INPP4B protein expression correlates with decreased overall patient survival for both breast and ovarian cancers (Gewinner et al., 2009; Bertucci et al., 2013). In summary, genomic analysis revealed that the alterations seen in the murine models are similar to those observed in human tumors, indicating that these models successfully recapitulate the genomic alteration profile of human HGSCs.

Discussion

Resolving the site of origin for high-grade serous ovarian carcinomas is integral to devising optimal strategies for risk reduction in high-risk women (Collins et al., 2011). Similarly, determining precisely where these tumors initiate will influence strategies for early detection. This includes the development of screening tests using novel serum tumor markers and improved methods of diagnostic imaging that focus on the distal FTE, in addition to the ovary. However, achieving these goals requires a model that accurately mimics the human disease. While several animal models of ovarian cancer have recently been reported, none target the clinically relevant FTSEC. In this study, we successfully generated a *de novo* mouse model of HGSC that targets commonly altered HGSC genes specifically to secretory epithelial cells within the fallopian tube. Interestingly, when using the *Pax8* promoter to drive *Cre*-mediated recombination of *Brca1* or *Brca2*, *Tp53*, and *Pten* in FTSECs, we observe the development of precursor STIC lesions, HGSC, and the progression to advanced stage disease, including ovarian and peritoneal metastases. By targeting genes that are commonly altered in human HGSC (TCGA, 2011), we have generated a murine model system that is highly clinically relevant.

To date, while it is still unclear if we can define a single cell of origin for HGSCs, our models serve as a proof-of-concept that high-grade serous “ovarian” tumors can arise from FTSECs and progress to metastatic disease via pre-invasive lesions, namely STICs. Interestingly, despite the fact that the mice displayed STIC lesions, the FT appeared normal on gross inspection in the majority of cases, while the ovary often showed visible signs of

disease. This observation is made repeatedly in the examination of human specimens and may shed light on the propensity to term this disease “ovarian” cancer. Importantly, the unique ability of our murine tumors to accurately recapitulate the histologic, immunophenotypic, and genomic alterations observed in human HGSC, provides a compelling argument for serous carcinogenesis originating in the FTSEC. Specifically, the tumors expressed key tumor and serum proteins, including CK-8, STMN1, PAX2, P53, Ki-67, WT1, and CA-125, all of which are used clinically in the assessment of ovarian tumors. In addition, our genomic analysis revealed that the alterations seen in murine tumors are indeed similar to those observed in corresponding HGSC patients (TCGA, 2011), such as amplifications of the *c-Myc* locus, and copy number alterations in DNA damage, HR-mediated repair, Notch, PI3K/KRAS, and cell cycle-related genes, indicating that these models faithfully recapitulate human HGSC pathogenesis.

TP53 mutations are one of the hallmarks of HGSC (TCGA, 2011) (Ahmed et al., 2010) and widely disseminated disease is likely to harbor dominant negative and/or loss of function mutations at the *TP53* locus (Sood et al., 1999). However, although *TP53* mutations appear to be obligatory in HGSC, to date little is known about the ability of TP53 to drive ovarian cancer. In our models, there was no obvious phenotypic difference between tumors with complete deletion of *Tp53* and tumors expressing a $Tp53^{R270H}$ dominant negative mutation. Interestingly, *Tp53* mutations coupled with loss of *Pten* did not drive progression of the disease beyond the initial pre-invasive stage in our mice, even well beyond the timeline when we saw widespread peritoneal disease with the additional targeting of *Brca1* or *Brca2*. This observation supports clinical data that *TP53* mutations alone rarely drive ovarian tumor formation (Nichols et al., 2001) but suggests that *PTEN* loss, a frequent occurrence in human STICs (Roh et al., 2010), can cooperate with mutant *TP53* in early serous tumorigenesis. Future studies will focus on understanding the clinical implications of *Tp53* loss versus expression of various different *Tp53* mutants in the development of HGSC. Collectively, the murine and human data indicate that alterations in *PTEN* or the PTEN/PI3K pathway are important in the development of STIC lesions and FTSEC malignant transformation. Furthermore, our data suggest that the *BRCA* status may play a much more significant role in the development of metastatic HGSC despite it being altered much less frequently than *TP53* in human HGSC cases (Alsop et al., 2012; TCGA, 2011). Previous studies have shown that cells with loss of expression in *BRCA1* or *BRCA2* genes have defective HR-mediated repair pathways and are likely candidates for PARP inhibitors (Farmer et al., 2005; Fong et al., 2009; Veeck et al., 2010). It has recently been suggested that other genetic alterations, including *EMSY* mutations, deletion or mutation of *PTEN* and *INPP4B* genes, *ATM* or *ATR* mutations, and Fanconi anemia gene mutations, may render cells sensitive to PARP inhibition; however, this has not been tested in an experimental *in vivo* model. Our models, which have shown many of these genetic alterations, allow for an elegant system in which to test the efficacy of PARP inhibitors. Furthermore, these models will allow us to investigate in a pre-clinical setting whether tumors with *BRCA2* mutations have a more efficacious response to PARP inhibitors compared to *BRCA1* tumors.

Most importantly, early detection of HGSC is difficult but the concept is highly attractive because it can conceivably be achieved at less cost and burden to the patient. If a significant proportion of “ovarian” serous cancers actually emerge from the distal fallopian tube, a significant shift in both conceptual thinking and preventive strategy will be required. It will be important to determine if patients at high-risk for HGSC should only have the affected distal portion of the fallopian tube removed, rather than both tubes and ovaries. Can these young *BRCA* women be offered risk-reduction surgery without undergoing surgical menopause and loss of their fertility? Similarly, determining precisely where these tumors initiate will influence strategies for early detection. This includes the development of screening tests using novel serum tumor markers and improved methods of diagnostic

imaging that focus on the distal FTE in addition to the ovary. In conclusion, the first goal of our research has been to produce a valid model of serous high-grade tumors. The second is to identify unique characteristics of early serous carcinogenesis in the tube that can be exploited for early detection and to examine the causes of the earliest events preceding malignancy, which will create a great opportunity for cancer prevention in high-risk women. It is clear that events leading to the development of STICs play a significant role in the development of serous tumors. Resolving their pathogenesis will enable more efficient methods for early detection, tumor imaging, cancer prevention, and identification of populations at risk.

Experimental Procedures

Development of genetically engineered mouse models

All animal studies and procedures were approved by the Dana Farber Cancer Institute and Harvard Medical School Animal Care and Use Committees. *PAX8-rtTA, TetO-Cre, and Gt (ROSA) 26Sor* strains (C57Bl background) were acquired from the Jackson Laboratory (Perl et al., 2002; Soriano, 1999; Traykova-Brauch et al., 2008). *Brca1*$^{flox/flox}$ and *Brca2*$^{flox/flox}$ mice were generated by insertion of *LoxP* sites into introns surrounding exon 11 in the *Brca1* and *Brca2* loci respectively, on a stock background (Jonkers et al., 2001; Xu et al., 1999). For the *Tp53*$^{flox/flox}$ mice *LoxP* sites were inserted in introns 1 and 10 of the endogenous *Tp53* locus. *Tp53-LSL-R270H* (*Tp53*^{R270H}) mice contain a dominant negative point-mutant allele of *Tp53* that can be activated by *Cre*-mediated recombination (Olive et al., 2004). *Tp53*$^{flox/flox}$ and the *Tp53*^{R270H} mice were a gift from Dr. Tyler Jacks (MIT). *Pten*$^{flox/flox}$ mice were generated by inserting *LoxP* sites into the *Pten* locus flanking exon 5 (Lesche et al., 2002). Genotyping procedures are described in the Supplemental Experimental Procedures. In order to drive Cre-mediated recombination in murine FTSECs, we treated experimental and control mice for 14 days with Dox (Sigma) using a concentration of 0.2 mg/ml in their drinking water. Animals were routinely monitored for signs of distress, poor body condition, and tumor burden and were euthanized according to veterinary recommendations. For survival curve experiments, the mice were monitored until their death or upon veterinary recommendations.

Quantification of Serum CA-125 Levels

CA-125 levels in murine sera, which were collected via cardiac puncture during necropsy, were quantified using a USCN ELISA kit (Life Science Inc, Wuhan) according to manufacturer's instructions. 100 μl of serum was used per sample for ELISA testing.

Array Comparative Genomic Hybridization (aCGH)

Mouse genomic DNA was isolated using Gentra Puregene Cell Kit (Qiagen) according to the manufacturer's instructions. Array CGH was performed using whole genome Agilent SurePrint G3 mouse CGH 1M catalog array (Agilent Technologies Inc.). Genomic DNA from 3 normal mouse FTs was pooled and used as a reference. 1 μg of total genomic DNA from the reference and test samples (derived from murine HGSC tumors) was used to perform array CGH according to the manufacturer's protocol. Briefly, reference and test DNA were first fragmented using a heat block at 95°C for 5 min and then labeled with Cyanine 3/Cyanine 5 fluorescence-labeled nucleotides respectively, according to the BioPrime Array CGH Genomic Labeling protocol (Invitrogen). Labeled DNA was purified using Amicon® Ultra-0.5 30k purification columns (Millipore). Test and reference DNA were then combined and hybridized to the Agilent 1M mouse catalog array for 40 hr at 65°C. The array slides were further washed and scanned. Probe signal intensities were obtained using the feature extraction software analysis provided by Agilent. Copy number alterations were identified using Nexus software analysis (BioDiscovery). The FASST2

segmentation algorithm was applied by setting the following parameters: a minimum number of 5 probes per segment were used to detect a copy number aberration with a significance threshold of $5x10^{-6}$; we further used log ratio cut offs of ±0.3 to detect one copy gain/loss and ±0.7 to detect high gain/homozygous loss.

Comparison with the human TCGA dataset

Mouse and human orthology information was obtained from the Mouse Genome Informatics database (http://www.informatics.jax.org/mgihome/other/citation.shtml) (Eppig et al., 2012) using the mm9 mouse genome reference assembly. The resulting regions were then compared to the alterations identified in the TCGA dataset (The Cancer Genome Atlas Research Network, 2011). The syntax "<gene name>:CNA >= GAIN" and "<gene name>:CNA <= HETLOSS" were used to query single copy gains and losses from the TCGA cbio portal, respectively (Cerami et al., 2012).

Supplementary Material

Refer to Web version on PubMed Central for supplementary material.

Acknowledgments

The authors wish to thank Christine Lam, Mei Zheng, and Huiying Piao for excellent technical assistance and the members of the Dinulescu and Drapkin labs for helpful discussions. We thank Dr. Andrew Godwin (University of Kansas Medical Center) for the HIO cells. This work is supported by grants from NIH, SPORE P50 CA105009 (RD), EDRN U01 CA152990 (RD), R21 CA156021 (RD), DOD OCRP W81XWH-10-1-0263 award (DMD), American Cancer Society RSG-13-083-01-TBG award (DMD), Ovarian Cycle and Ovarian Cancer Research Fund Liz Tilberis award (DMD), Burroughs-Wellcome Fund Career Award in the Biomedical Sciences 1005320.01 (DMD), V Foundation for Cancer Research Scholar Award (DMD), Marsha Rivkin Foundation for Ovarian Cancer Research (DMD), the Mildred Moorman Ovarian Cancer Research Fund (DMD), Dr. Miriam and Sheldon G. Adelson Medical Research Foundation (RD), Ovarian Cancer Research Fund Ann Schreiber award (RP), the National Ovarian Cancer Coalition (RD, RP), the Mary Kay Foundation (RD, DMD), Sandy Rollman Ovarian Cancer Foundation (RD), the Susan Smith Center for Women's Cancers at the Dana-Farber Cancer Institute (RD, DMD), the Debra and Robert First Fund (RD), the Gamel Family Fund (RD), and the Eleanor and Miles Shore 50th Anniversary Fellowship Program for Scholars in Medicine Award (SRS).

References

Ahmed AA, Etemadmoghadam D, Temple J, Lynch AG, Riad M, Sharma R, Stewart C, Fereday S, Caldas C, Defazio A, Bowtell D, Brenton JD. Driver mutations in TP53 are ubiquitous in high grade serous carcinoma of the ovary. J Pathol. 2010; 221(1):49–56. [PubMed: 20229506]

Alsop K, Fereday S, Meldrum C, deFazio A, Emmanuel C, George J, Dobrovic A, Birrer MJ, Webb PM, Stewart C, et al. BRCA mutation frequency and patterns of treatment response in BRCA mutation-positive women with ovarian cancer: a report from the Australian Ovarian Cancer Study Group. J Clin Oncol. 2012; 30:2654–2663. [PubMed: 22711857]

Bast RC Jr. Status of tumor markers in ovarian cancer screening. J Clin Oncol. 2003; 21:200s–205s. [PubMed: 12743135]

Bertucci MC, Mitchell CA. Phosphoinositide 3-kinase and INPP4B in human breast cancer. Ann NY Acad Sci. 2013; 1280:1–5. [PubMed: 23551093]

Bowen NJ, Logani S, Dickerson EB, Kapa LB, Akhtar M, Benigno BB, McDonald JF. Emerging roles for PAX8 in ovarian cancer and endosalpingeal development. Gynecol Oncol. 2007; 104:331–337. [PubMed: 17064757]

Cerami E, Gao J, Dogrusoz U, Gross BE, Sumer SO, Aksoy BA, Jacobsen A, Byrne CJ, Heuer ML, Larsson E, et al. The cBio cancer genomics portal: an open platform for exploring multidimensional cancer genomics data. Cancer Discovery. 2012; 2:401–404. [PubMed: 22588877]

Chene G, Tchirkov A, Pierre-Eymard E, Dauplat J, Raoelfils I, Cayre A, Watkin E, Vago P, Penault-Llorca F. Early telomere shortening and genomic instability in tubo-ovarian preneoplastic lesions. Clin Cancer Res. 2013; 19(11):2873–82. [PubMed: 23589176]

Cheung HW, Cowley GS, Weir BA, Boehm JS, Rusin S, Scott JA, East A, Ali LD, Lizotte PH, Wong TC, et al. Systematic investigation of genetic vulnerabilities across cancer cell lines reveals lineage-specific dependencies in ovarian cancer. Proc Natl Acad Sci U S A. 2011; 108:12372–12377. [PubMed: 21746896]

Clark-Knowles KV, Garson K, Jonkers J, Vanderhyden BC. Conditional inactivation of Brca1 in the mouse ovarian surface epithelium results in an increase in preneoplastic changes. Exp Cell Res. 2007; 313:133–145. [PubMed: 17070800]

Clark-Knowles KV, Senterman MK, Collins O, Vanderhyden BC. Conditional inactivation of Brca1, p53 and Rb in mouse ovaries results in the development of leiomyosarcomas. PLoS One. 2009; 4:e8534. [PubMed: 20046869]

Collins IM, Domchek SM, Huntsman DG, Mitchell G. The tubal hypothesis of ovarian cancer: caution needed. Lancet Oncol. 2011; 12:1089–1091. [PubMed: 21868285]

Dinulescu DM, Ince TA, Quade BJ, Shafer SA, Crowley D, Jacks T. Role of K-ras and Pten in the development of mouse models of endometriosis and endometrioid ovarian cancer. Nat Med. 2005; 11:63–70. [PubMed: 15619626]

Eppig JT, Blake JA, Bult CJ, Kadin JA, Richardson JE. The Mouse Genome Database (MGD): comprehensive resource for genetics and genomics of the laboratory mouse. Nucleic Acids Res. 2012; 40:D881–886. [PubMed: 22075990]

Farmer H, McCabe N, Lord CJ, Tutt AN, Johnson DA, Richardson TB, Santarosa M, Dillon KJ, Hickson I, Knights C, et al. Targeting the DNA repair defect in BRCA mutant cells as a therapeutic strategy. Nature. 2005; 434:917–921. [PubMed: 15829967]

Flesken-Nikitin A, Choi KC, Eng JP, Shmidt EN, Nikitin AY. Induction of carcinogenesis by concurrent inactivation of p53 and Rb1 in the mouse ovarian surface epithelium. Cancer Res. 2003; 63:3459–3463. [PubMed: 12839925]

Flesken-Nikitin A, Hwang CI, Cheng CY, Michurina TV, Enikolopov G, Nikitin AY. Ovarian surface epithelium at the junction area contains a cancer-prone stem cell niche. Nature. 2013; 395:241–245. [PubMed: 23467088]

Folkins AK, Jarboe EA, Saleemuddin A, Lee Y, Callahan MJ, Drapkin R, Garber JE, Muto MG, Tworoger S, Crum CP. A candidate precursor to pelvic serous cancer (p53 signature) and its prevalence in ovaries and fallopian tubes from women with BRCA mutations. Gynecol Oncol. 2008; 109:168–173. [PubMed: 18342932]

Fong PC, Boss DS, Yap TA, Tutt A, Wu P, Mergui-Roelvink M, Mortimer P, Swaisland H, Lau A, O'Connor MJ, et al. Inhibition of poly(ADP-ribose) polymerase in tumors from BRCA mutation carriers. N Engl J Med. 2009; 361:123–134. [PubMed: 19553641]

Gewinner C, Wang ZC, Richardson A, Teruya-Feldstein J, Etemadmoghadam D, Bowtell D, Barretina J, Lin WM, Rameh L, Salmena L, et al. Evidence that inositol polyphosphate 4-phosphatase type II is a tumor suppressor that inhibits PI3K signaling. Cancer Cell. 2009; 16(2):115–125. [PubMed: 19647222]

Jazaeri AA, Bryant JL, Park H, Li H, Dahiya N, Stoler MH, Ferriss JS, Dutta A. Molecular requirements for transformation of fallopian tube epithelial cells into serous carcinoma. Neoplasia. 2011; 13(10):899–911. [PubMed: 22028616]

Jonkers J, Meuwissen R, van der Gulden H, Peterse H, van der Valk M, Berns A. Synergistic tumor suppressor activity of BRCA2 and p53 in a conditional mouse model for breast cancer. Nature genetics. 2001; 29:418–425. [PubMed: 11694875]

Karst AM, Levanon K, Drapkin R. Modeling high-grade serous ovarian carcinogenesis from the fallopian tube. Proc Natl Acad Sci U S A. 2011a; 108:7547–7552. [PubMed: 21502498]

Karst AM, Levanon K, Duraisamy S, Liu JF, Hirsch MS, Hecht JL, Drapkin R. Stathmin 1, a marker of PI3K pathway activation and regulator of microtubule dynamics, is expressed in early pelvic serous carcinomas. Gynecol Oncol. 2011b; 123:5–12. [PubMed: 21683992]

Kim J, Coffey DM, Creighton CJ, Yu Z, Hawkins SM, Matzuk MM. High-grade serous ovarian cancer arises from fallopian tube in a mouse model. Proc Natl Acad Sci U S A. 2012; 109:3921–3926. [PubMed: 22331912]

Kindelberger DW, Lee Y, Miron A, Hirsch MS, Feltmate C, Medeiros F, Callahan MJ, Garner EO, Gordon RW, Birch C, et al. Intraepithelial carcinoma of the fimbria and pelvic serous carcinoma: Evidence for a causal relationship. Am J Surg Pathol. 2007; 31:161–169. [PubMed: 17255760]

Kinross KM, Montgomery KG, Kleinschmidt M, Waring P, Ivetac I, Tikoo A, Saad M, Hare L, Roh V, Mantamadiotis T, et al. An activating Pik3ca mutation coupled with Pten loss is sufficient to initiate ovarian tumorigenesis in mice. J Clin Invest. 2012; 122(2):553–557. [PubMed: 22214849]

Kuhn E, Meeker AK, Visvanathan K, Gross AL, Wang TL, Kurman RJ, Shih Ie M. Telomere length in different histologic types of ovarian carcinoma with emphasis on clear cell carcinoma. Mod Pathol. 2011; 24:1139–1145. [PubMed: 21499239]

Laury AR, Hornick JL, Perets R, Krane JF, Corson J, Drapkin R, Hirsch MS. PAX8 reliably distinguishes ovarian serous tumors from malignant mesothelioma. Am J Surg Pathol. 2010; 34:627–635. [PubMed: 20414098]

Laury AR, Perets R, Piao H, Krane JF, Barletta JA, French C, Chirieac LR, Lis R, Loda M, Hornick JL, et al. A comprehensive analysis of PAX8 expression in human epithelial tumors. The American journal of surgical pathology. 2011; 35:816–826. [PubMed: 21552115]

Lee Y, Miron A, Drapkin R, Nucci MR, Medeiros F, Saleemuddin A, Garber J, Birch C, Mou H, Gordon RW, et al. A candidate precursor to serous carcinoma that originates in the distal fallopian tube. J Pathol. 2007; 211:26–35. [PubMed: 17117391]

Leeper K, Garcia R, Swisher E, Goff B, Greer B, Paley P. Pathologic findings in prophylactic oophorectomy specimens in high-risk women. Gynecol Oncol. 2002; 87:52–56. [PubMed: 12468342]

Lesche R, Groszer M, Gao J, Wang Y, Messing A, Sun H, Liu X, Wu H. Cre/loxP-mediated inactivation of the murine Pten tumor suppressor gene. Genesis. 2002; 32:148–149. [PubMed: 11857804]

Levanon K, Crum C, Drapkin R. New insights into the pathogenesis of serous ovarian cancer and its clinical impact. J Clin Oncol. 2008; 26:5284–5293. [PubMed: 18854563]

Medeiros F, Muto MG, Lee Y, Elvin JA, Callahan MJ, Feltmate C, Garber JE, Cramer DW, Crum CP. The tubal fimbria is a preferred site for early adenocarcinoma in women with familial ovarian cancer syndrome. Am J Surg Pathol. 2006; 30:230–236. [PubMed: 16434898]

Mittag J, Winterhager E, Bauer K, Grummer R. Congenital hypothyroid female pax8-deficient mice are infertile despite thyroid hormone replacement therapy. Endocrinology. 2007; 148:719–725. [PubMed: 17082261]

Mullany LK, Fan HY, Liu Z, White LD, Marshall A, Gunaratne P, Anderson ML, Creighton CJ, Xin L, Deavers M, et al. Molecular and functional characteristics of ovarian surface epithelial cells transformed by KrasG12D and loss of Pten in a mouse model in vivo. Oncogene. 2011; 30:3522–3536. [PubMed: 21423204]

Mutter GL, Lin MC, Fitzgerald JT, Kum JB, Baak JP, Lees JA, Weng LP, Eng C. Altered PTEN expression as a diagnostic marker for the earliest endometrial precancers. J Natl Cancer Inst. 2000; 92:924–930. [PubMed: 10841828]

Nichols KE, Malkin D, Garber JE, Fraumeni JF Jr, Li FP. Germ-line p53 mutations predispose to a wide spectrum of early-onset cancers. Cancer epidemiology, biomarkers & prevention : a publication of the American Association for Cancer Research, cosponsored by the American Society of Preventive Oncology. 2001; 10:83–87.

Olive KP, Tuveson DA, Ruhe ZC, Yin B, Willis NA, Bronson RT, Crowley D, Jacks T. Mutant p53 gain of function in two mouse models of Li-Fraumeni syndrome. Cell. 2004; 119:847–860. [PubMed: 15607980]

Perl AK, Wert SE, Nagy A, Lobe CG, Whitsett JA. Early restriction of peripheral and proximal cell lineages during formation of the lung. Proc Natl Acad Sci U S A. 2002; 99:10482–10487. [PubMed: 12145322]

Przybycin CG, Kurman RJ, Ronnett BM, Shih Ie M, Vang R. Are all pelvic (nonuterine) serous carcinomas of tubal origin? Am J Surg Pathol. 2010; 34:1407–1416. [PubMed: 20861711]

Quinn BA, Brake T, Hua X, Baxter-Jones K, Litwin S, Ellenson LH, Connolly DC. Induction of ovarian leiomyosarcomas in mice by conditional inactivation of Brca1 and p53. PLoS One. 2009; 4:e8404. [PubMed: 20046879]

Roh MH, Yassin Y, Miron A, Mehra KK, Mehrad M, Monte NM, Mutter GL, Nucci MR, Ning G, Mckeon FD, et al. High-grade fimbrial-ovarian carcinomas are unified by altered p53, PTEN and PAX2 expression. Mod Pathol. 2010; 23(10):1316–1324. [PubMed: 20562848]

Siegel R, Naishadham D, Jemal A. Cancer statistics, 2012. CA Cancer J Clin. 2012; 62:10–29. [PubMed: 22237781]

Sood AK, Sorosky JI, Dolan M, Anderson B, Buller RE. Distant metastases in ovarian cancer: association with p53 mutations. Clin Cancer Res. 1999; 5:2485–2490. [PubMed: 10499623]

Soriano P. Generalized lacZ expression with the ROSA26 Cre reporter strain. Nat Genet. 1999; 21:70–71. [PubMed: 9916792]

Szabova L, Yin C, Bupp S, Guerin TM, Schlomer JJ, Householder DB, Baran ML, Yi M, Song Y, Sun W, et al. Perturbation of Rb, p53, and Brca1 or Brca2 cooperate in inducing metastatic serous epithelial ovarian cancer. Cancer Res. 2012; 72:4141–4153. [PubMed: 22617326]

Tacha D, Zhou D, Cheng L. Expression of PAX8 in normal and neoplastic tissues: a comprehensive immunohistochemical study. Appl Immunohistochem Mol Morphol. 2011; 19:293–299. [PubMed: 21285870]

TCGA. Integrated genomic analyses of ovarian carcinoma. Nature. 2011; 474:609–615. [PubMed: 21720365]

Traykova-Brauch M, Schonig K, Greiner O, Miloud T, Jauch A, Bode M, Felsher DW, Glick AB, Kwiatkowski DJ, Bujard H, et al. An efficient and versatile system for acute and chronic modulation of renal tubular function in transgenic mice. Nat Med. 2008; 14:979–984. [PubMed: 18724376]

Vaughan S, Coward JI, Bast RC Jr, Berchuck A, Berek JS, Brenton JD, Coukos G, Crum CC, Drapkin R, Etemadmoghadam D, et al. Rethinking ovarian cancer: recommendations for improving outcomes. Nat Rev Cancer. 2011; 11:719–725. [PubMed: 21941283]

Veeck J, Ropero S, Setien F, Gonzalez-Suarez E, Osorio A, Benitez J, Herman JG, Esteller M. BRCA1 CpG island hypermethylation predicts sensitivity to poly(adenosine diphosphate)-ribose polymerase inhibitors. J Clin Oncol. 2010; 28:e563–564. author reply e565–566. [PubMed: 20679605]

Wu R, Baker SJ, Hu TC, Norman KM, Fearon ER, Cho KR. Type I to type II ovarian carcinoma progression: mutant Trp53 or Pik3ca confers a more aggressive tumor phenotype in a mouse model of ovarian cancer. Am J Pathol. 2013; 182:1391–399. [PubMed: 23499052]

Wu R, Hendrix-Lucas N, Kuick R, Zhai Y, Schwartz DR, Akyol A, Hanash S, Misek DE, Katabuchi H, Williams BO, et al. Mouse model of human ovarian endometrioid adenocarcinoma based on somatic defects in the Wnt/beta-catenin and PI3K/Pten signaling pathways. Cancer Cell. 2007; 11:321–333. [PubMed: 17418409]

Xu X, Wagner KU, Larson D, Weaver Z, Li C, Ried T, Hennighausen L, Wynshaw-Boris A, Deng CX. Conditional mutation of Brca1 in mammary epithelial cells results in blunted ductal morphogenesis and tumour formation. Nat Genet. 1999; 22:37–43. [PubMed: 10319859]

Highlights

- PAX8 can drive murine high-grade serous tumors originating in the fallopian tube
- Early alterations in *Brca*, *Tp53*, and *Pten* lead to intraepithelial precursor lesions
- Genomic analysis of *Pax8*-driven tumors shows strong correlation with human tumors
- High-grade serous ovarian cancer can arise from the fallopian tubal secretory cell

Significance

Recent histological studies suggest that many serous carcinomas can arise from intraepithelial lesions in the fallopian tube. This is based largely on association studies and has never been proven due to lack of effective early detection methods in patients and the shortage of valid experimental models. Herein, we present a genetic model of *de novo* high-grade serous carcinoma (HGSC) that originates in fallopian tubal secretory epithelial cells and recapitulates the key genetic alterations and precursor lesions characteristic of human invasive ovarian cancer. In addition to offering mechanistic insight into the origin and pathogenesis of HGSC, this model provides a platform to explore HGSC sensitivity to novel therapeutic strategies and to develop better early detection strategies for women at risk.

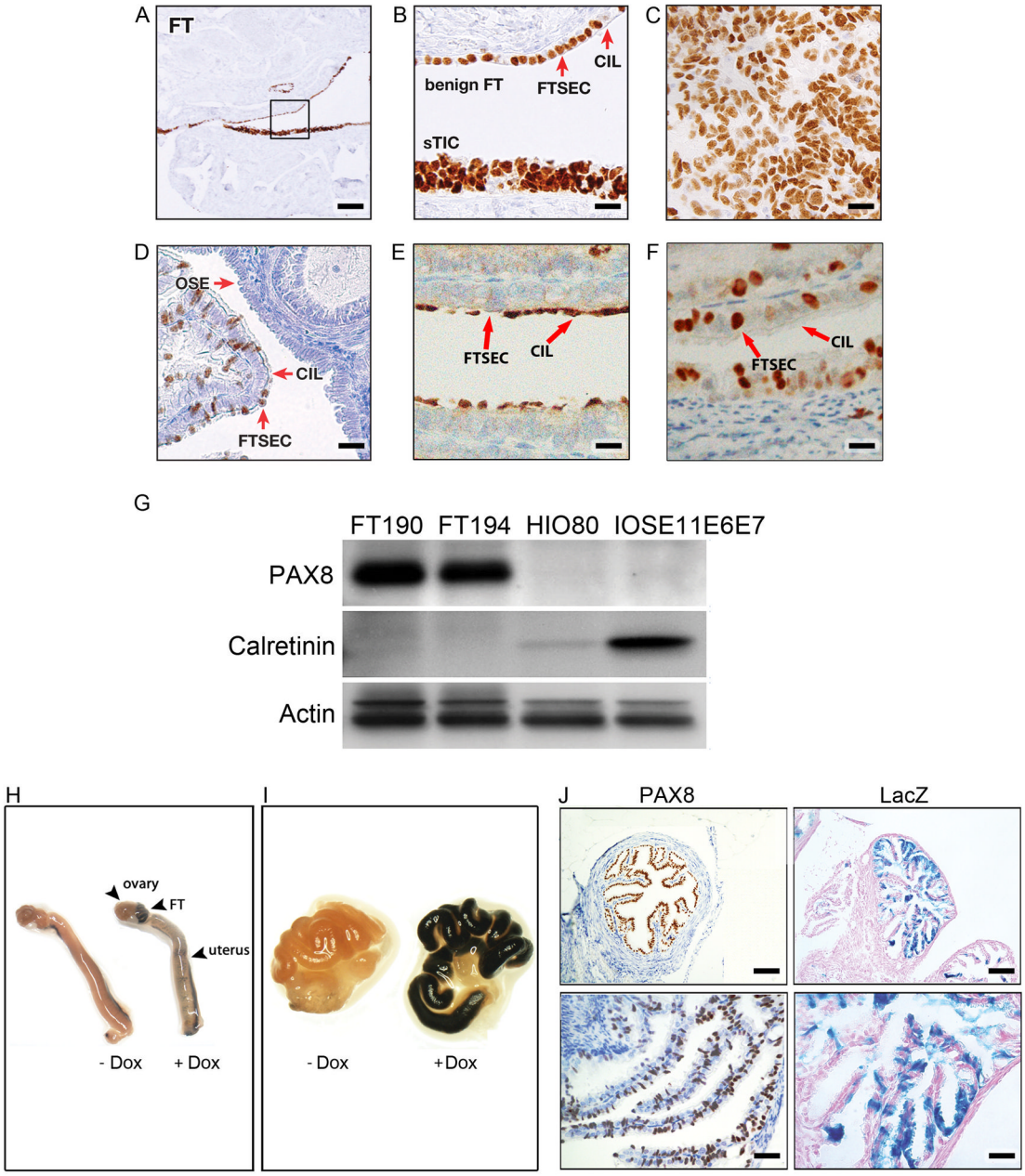

Figure 1. Expression of PAX8, a specific Müllerian lineage marker, during FT malignant transformation

(A, B) Immunohistochemistry (IHC) for PAX8 in the human FTE is shown for the benign epithelium (top) and STIC (bottom). The square area in (A) is shown at a higher magnification in (B). PAX8 positive FTSEC and PAX8-negative ciliated cells (CIL) are demarcated by red arrows. (C) IHC for PAX8 in human HGSC. (D) PAX8 expression in mouse OSE, CIL cells, and FTSECs. (E) IHC for acetylated tubulin in mouse CIL cells and FTSEC. (F) PAX8 expression in murine non-ciliated FTSECs. (G) PAX8 and calretinin expression in immortalized FTSEC lines (FT190 and FT194) and in HOSE cell lines (HIO-80 and IOSE11E6E7) as depicted by Western Blot analysis. Calretinin is used as a marker for HOSE and β-actin serves as a loading control. (H) Gross anatomy of murine female genital tracts collected from *Pax8-rtTA;TetO-Cre;LSL-LacZ* mice treated (+Dox) or

untreated (−Dox) with Dox and stained with a β-galactosidase stain. (I) Higher magnification of the FT treated or untreated with Dox. (J) Non-neoplastic mouse FTE stained with PAX8 or LacZ as indicated. Scale bars: 500 μm (A), 50 μm (B–F), 100 μm (J, top subpanels), and 33.3 μm (J, bottom subpanels). See also Figure S1.

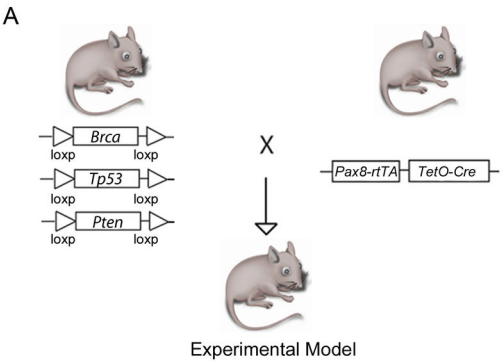

B

Genotype	Number of Mice	Survival (weeks)	STIC	FT Transformation	Ovarian Metastasis	Peritoneal Metastasis
Brca1$^{-/-}$;Tp53^{mut};Pten$^{-/-}$;Pax8-rtTA;TetO-Cre	4	5-17	4/4 (100%)	4/4 (100%)	1/4* (25%)	1/4* (25%)
Brca1$^{+/-}$;Tp53^{mut};Pten$^{-/-}$;Pax8-rtTA;TetO-Cre	12	9-20	10/12 (83%)	10/12 (83%)	6/12 (50%)	8/12 (67%)
Brca2$^{-/-}$;Tp53^{mut};Pten$^{-/-}$;Pax8-rtTA;TetO-Cre	12	7-15	9/12 (75%)	9/12 (75%)	9/12 (75%)	8/12 (67%)
Brca2$^{+/-}$;Tp53^{mut};Pten$^{-/-}$;Pax8-rtTA;TetO-Cre	3	17-18	3/3 (100%)	3/3 (100%)	3/3 (100%)	2/3 (67%)
Tp53$^{-/-}$;Pten$^{-/-}$;Pax8-rtTA;TetO-Cre	6	19-38	4/6 (67%)	4/6 (67%)	0/6 (0%)	0/6 (0%)

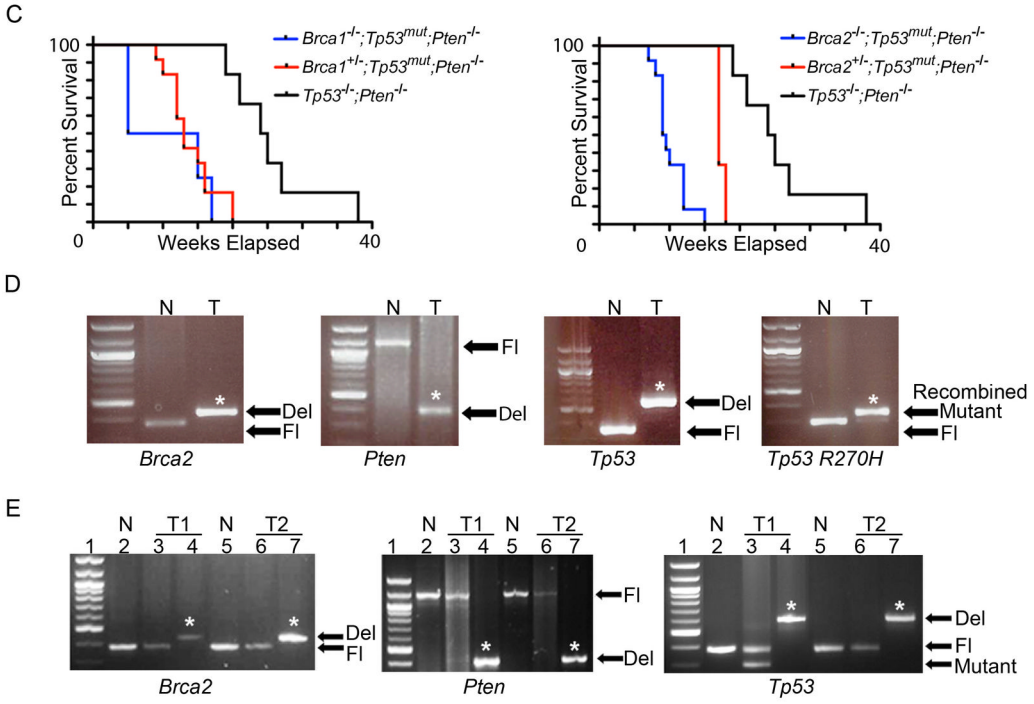

Figure 2. The role of *Brca*, *Tp53*, and *Pten* genetic alterations in the development of STIC, HGSC, and tumor metastases in *Pax8-Cre* mice

(A) Schematic representation of conditional *Brca1*, *Brca2*, *Tp53*, *Pten* alleles and *Pax8-rtTA;TetO-Cre* recombination. (B) Summary of the phenotypic characteristics of the 5 *Pax8-Cre* cohorts: *Brca1$^{-/-}$;Tp53^{mut};Pten$^{-/-}$*, *Brca1$^{+/-}$;Tp53^{mut};Pten$^{-/-}$*, *Brca2$^{-/-}$;Tp53^{mut};Pten$^{-/-}$*, *Brca2$^{+/-}$;Tp53^{mut};Pten$^{-/-}$*, and *Tp53$^{-/-}$;Pten$^{-/-}$* mice. The asterisk (*) denotes that 2 of the 4 *Brca1$^{-/-}$;Tp53^{mut};Pten$^{-/-}$* mice had to be sacrificed earlier at 5 weeks due to unrelated skin lesions in accordance to veterinarian recommendations, and as a result did not have time to develop metastatic disease. The *Brca1$^{-/-}$;Tp53^{mut};Pten$^{-/-}$* cohort includes 2 *Brca1$^{-/-}$;Tp53$^{-/-}$;Pten$^{-/-}$* and 2

Brca1$^{-/-}$;*Tp53*$^{R270H/-}$;*Pten*$^{-/-}$ mice. The *Brca1*$^{+/-}$;*Tp53*^{mut} ;*Pten*$^{-/-}$ cohort includes 8 *Brca1*$^{+/-}$;*Tp53*$^{-/-}$;*Pten*$^{-/-}$ and 4 *Brca1*$^{+/-}$;*Tp53*$^{R270H/-}$;*Pten*$^{-/-}$ animals. The *Brca2*$^{-/-}$;*Tp53*^{mut};*Pten*$^{-/-}$ cohort includes 6 *Brca2*$^{-/-}$;*Tp53*$^{-/-}$;*Pten*$^{-/-}$ and 6 *Brca2*$^{-/-}$;*Tp53*$^{R270H/-}$;*Pten*$^{-/-}$ mice. The *Brca2*$^{+/-}$;*Tp53*^{mut};*Pten*$^{-/-}$ cohort includes 2 *Brca2*$^{+/-}$;*Tp53*$^{-/-}$;*Pten*$^{-/-}$ and 1 *Brca2*$^{+/-}$;*Tp53*$^{R270H/-}$;*Pten*$^{-/-}$ animals. (C) Kaplan-Meier analysis of overall survival of all mouse cohorts. $p < 0.01$ comparing with and without deletion of any alleles of *Brca1* or *Brca2*. Statistical analysis was calculated using a log-rank analysis. (D) PCR reaction illustrating Cre-mediated recombination of *Brca2*, *Pten*, and *Tp53* alleles. T, DNA isolated from a *Brca2*$^{-/-}$;*Tp53*$^{R270H/-}$;*Pten*$^{-/-}$ HGSC tumor; N, unrecombined DNA; Fl, unrecombined floxed alleles; Del, deleted alleles; Mutant, *Tp53*^{R207H} allele. The asterisk (*) denotes recombined (deleted or mutant) bands. (E) Efficiency of Cre-mediated recombination for *Brca2*, *Pten*, and *Tp53* alleles, respectively, in HGSC tumors isolated from *Brca2*$^{-/-}$;*Tp53*$^{R270H/-}$;*Pten*$^{-/-}$ (T1) and *Brca2*$^{-/-}$;*Tp53*$^{-/-}$;*Pten*$^{-/-}$ (T2) mice as assayed by PCR. Lanes 2 and 5 (N) indicate control unrecombined DNA, lanes 3 (T1) and 6 (T2) indicate the level of unrecombined DNA in tumor cells, and lanes 4 (T1) and 7 (T2) show the level of recombined DNA in tumors. The asterisk (*) denotes recombined (deleted) bands. See also Figure S2, Tables S1, S2.

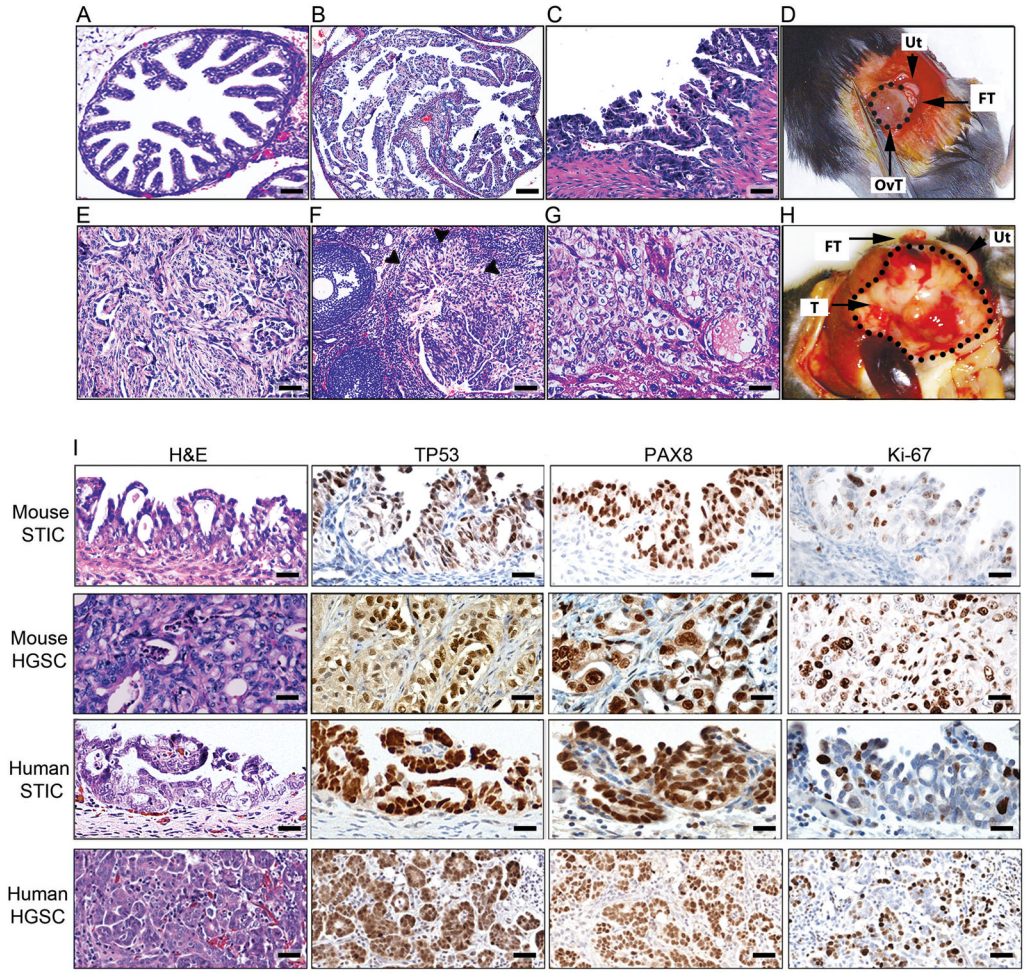

Figure 3. Characterization of the morphology and dissemination patterns of murine STICs and HGSCs in *Brca2* murine cohorts

(A) Cross-section of normal FT from a control wild-type mouse. (B, C) Examples of *Brca2*$^{-/-}$;*Tp53*$^{R270H/-}$;*Pten*$^{-/-}$ STICs. (D) Gross anatomy of a *Brca2*$^{+/-}$;*Tp53*$^{R270H/-}$;*Pten*$^{-/-}$ HGSC originating in the fallopian tube (FT) and metastasizing to the ovary (circled, OvT). Uterus (Ut) is shown as a reference. (E) Representative pictures of disseminated intraperitoneal *Brca2*$^{+/-}$;*Tp53*$^{R270H/-}$;*Pten*$^{-/-}$ tumors. (F) Representative pictures of metastases from *Brca2*$^{+/-}$;*Tp53*$^{R270H/-}$;*Pten*$^{-/-}$ HGSCs to the ovarian cortex in close proximity to the ovarian stalk. Tumor border is marked by arrowheads. (G) Examples of metastases from *Brca2*$^{+/-}$;*Tp53*$^{R270H/-}$;*Pten*$^{-/-}$ tumors to the liver. (H) Gross anatomy of a *Brca2*$^{+/-}$;*Tp53*$^{R270H/-}$;*Pten*$^{-/-}$ HGSC tumor originating in the fallopian tube (FT) and metastasizing to the peritoneal cavity (circled, T). (I) Comparative study of representative examples of murine *Brca2*$^{+/-}$;*Tp53*$^{R270H/-}$;*Pten*$^{-/-}$ tumor lesions and human STICs and HGSCs. Tissue sections were stained with H&E or stained for TP53, PAX8, or Ki-67, as indicated. Scale bars: 200 μm (A, B, F), 50 μm (C, I as shown in mouse STIC IHC, mouse HGSC, and human STIC subpanels), 100 μm (E, G, I as shown in mouse STIC H&E and human HGSC subpanels).

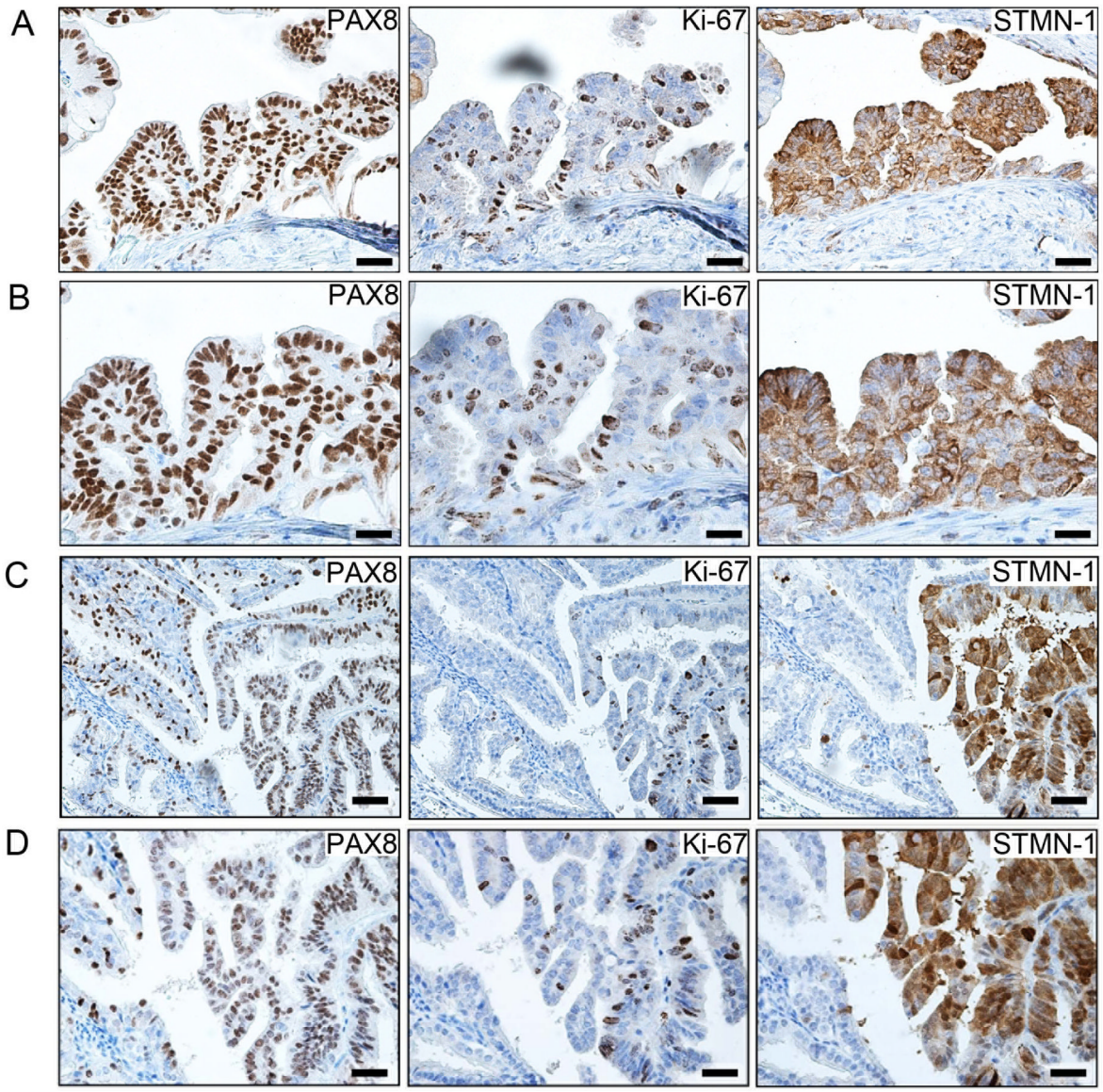

Figure 4. STMN1 expression in murine STIC lesions

(A, B) Representative low (A) and high (B) magnification images of immunohistochemical analysis for PAX8, Ki-67, and STMN1 markers in murine *Brca2*$^{-/-}$;*Tp53*$^{-/-}$;*Pten*$^{-/-}$ STIC lesions. (C, D) Representative low (C) and high (D) magnification images of immunohistochemical analysis for PAX8, Ki-67, and STMN1 in early murine *Brca2*$^{-/-}$;*Tp53*$^{-/-}$;*Pten*$^{-/-}$ tumor STIC lesion in the distal FT. Normal distal tube (fimbria) can be seen on the left side of the image. Scale bars: 100 μm (A, C) and 50 μm (B, D).

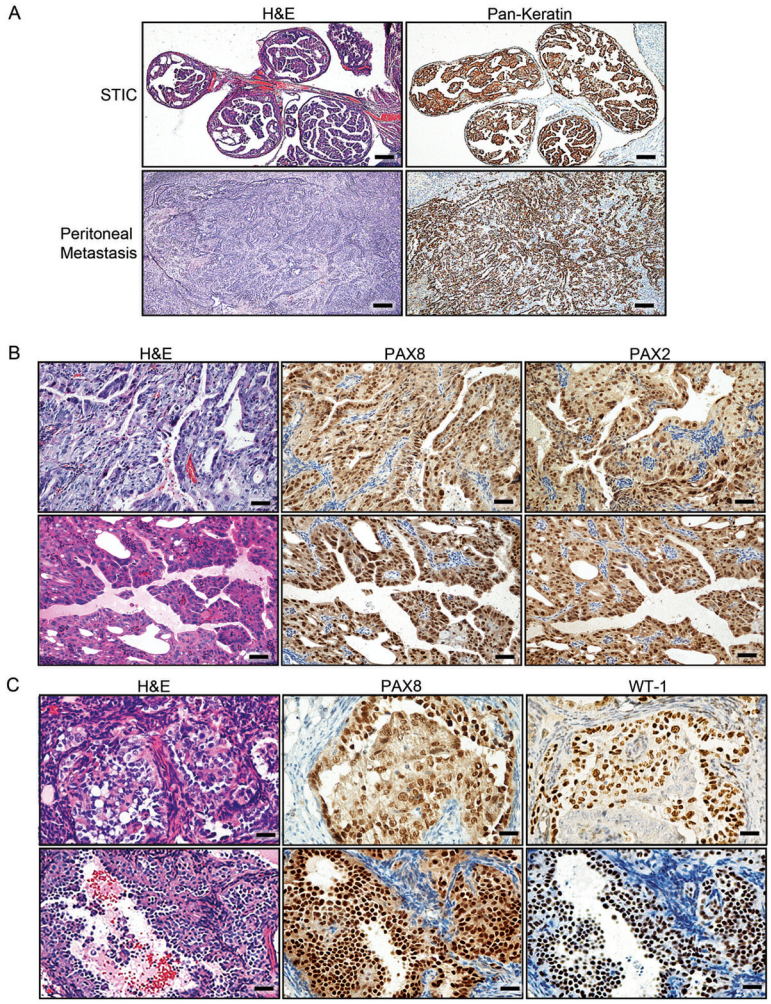

Figure 5. Immunohistochemical analysis for epithelial and HGSC markers in murine serous tumors

(A) Staining of STICs and invasive tumors for Pan-Keratin in *Brca1*$^{+/-}$;*Tp53*$^{-/-}$;*Pten*$^{-/-}$ tumors. (B) Examples of PAX8 and PAX2 staining in *Brca1*$^{+/-}$;*Tp53*$^{-/-}$;*Pten*$^{-/-}$ tumor lesions metastatic to the ovary. (C) Representative examples of PAX8 and WT1 staining in *Brca2*$^{-/-}$;*Tp53*$^{R270H/-}$;*Pten*$^{-/-}$ tumor lesions metastatic to the ovary. Scale bars: 500 μm (A), 100 μm (B), and 50 μm (C). See also Figure S3.

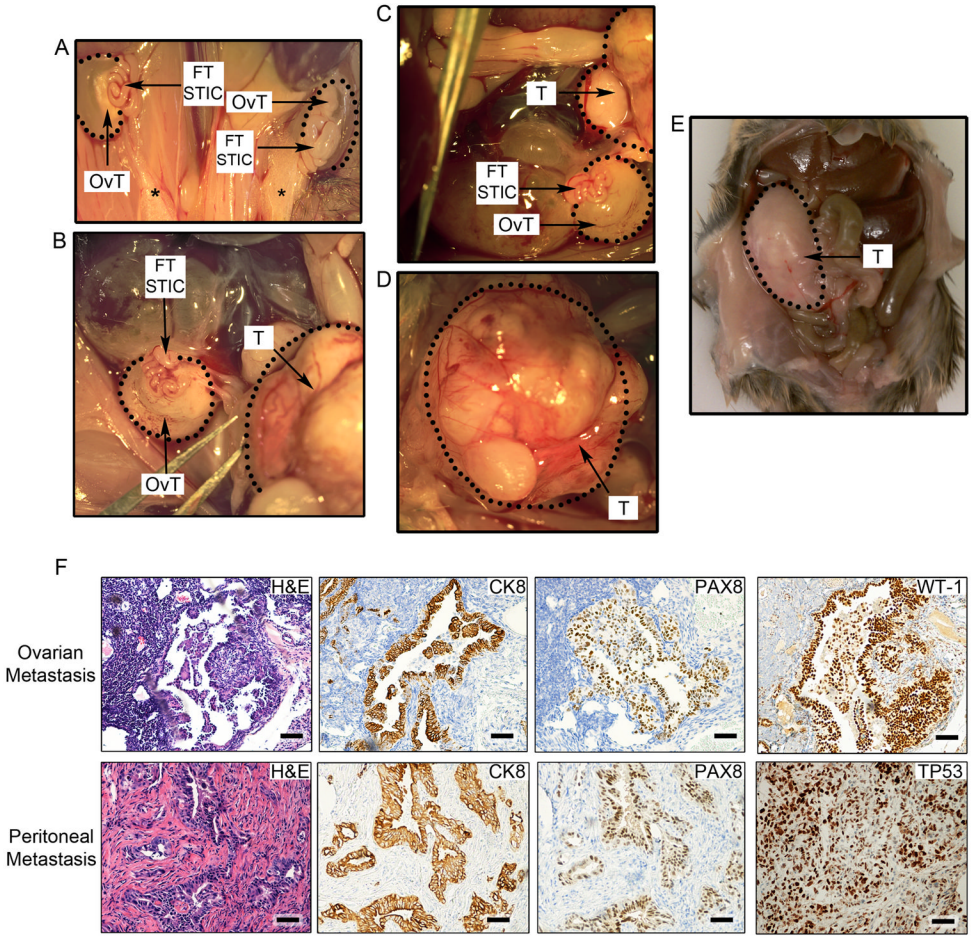

Figure 6. Hysterectomy, salpingectomy, and oophorectomy experiments to assess the origins of HGSCs

(A–E) Representative gross anatomy of tumor lesions found in mice undergoing hysterectomy. (A) Impact of hysterectomy on the development of bilateral ovarian HGSC tumors (OvT) originating in the fallopian tube (FT STIC) in a *Brca2*$^{-/-}$;*Tp53*$^{R270H/-}$;*Pten*$^{-/-}$ mouse. Black stars denote the removal of the uterus and the presence of the remaining fat deposits. FT STICs denote grossly normal appearing but histologically transformed fallopian tubes containing pre-invasive lesions. (B–D) Hysterectomy in a second *Brca1*$^{+/-}$;*Tp53*$^{-/-}$;*Pten*$^{-/-}$ mouse and the resultant HGSC metastasis to the ovary (encircled OvT) and peritoneum (encircled T). (D) The image depicts a higher magnification of the peritoneal HGSC metastasis (T). (E) Abdominal HGSC metastases (T) in a third *Brca2*$^{-/-}$;*Tp53*$^{R270H/-}$;*Pten*$^{-/-}$ mouse following hysterectomy. (F) Histopathological and immunohistochemical (CK8, PAX8, WT1, and TP53) analysis of ovarian (top subpanels) and peritoneal (bottom subpanels) HGSC metastases in murine models that underwent hysterectomy. Scale bars: 100 μm. See also Figure S4.

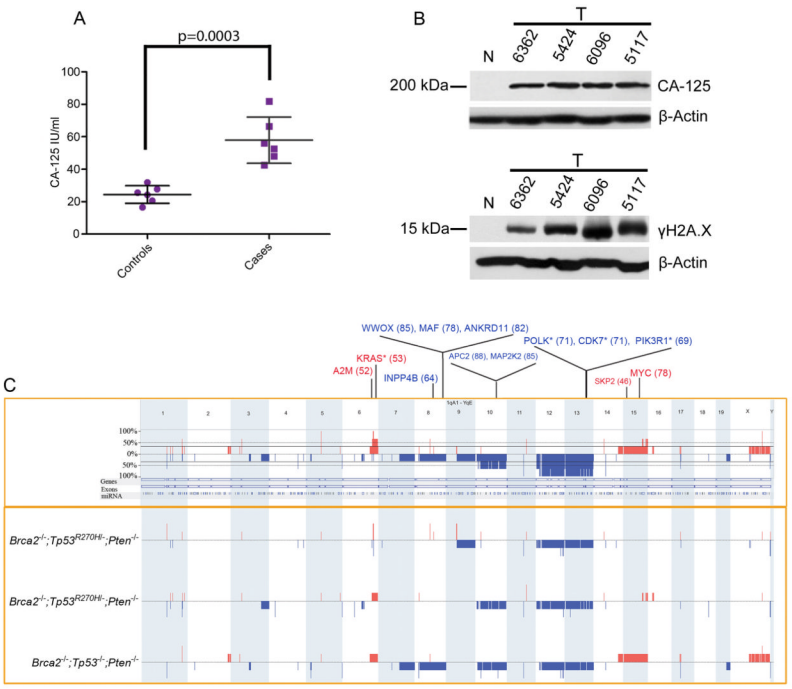

Figure 7. Serologic and genomic analyses of tumors from genetically engineered models

(A) Serum CA-125 levels in tumor-bearing mice (cases) compared to control animals. P-value was calculated using a two-tailed student's T-test. Error bars represent standard deviation. (B) Western Blot analysis for CA-125 and γH2A.X levels in 4 tumor samples isolated from *Brca1*$^{+/-}$*;Tp53*$^{-/-}$*;Pten*$^{-/-}$ (#6362 and #5424) and *Brca2*$^{-/-}$*;Tp53*$^{R270H/-}$*;Pten*$^{-/-}$ mice (#6096 and #5117) and compared to normal Dox-untreated FT (N). (C) Schematic representation of the genomic alterations found in murine HGSCs. Copy number losses and gains are shown in blue and red, respectively. The boxed upper panel depicts the frequency of the alterations including all murine tumors tested, while the boxed lower panel represents the alterations found in individual tumors. Key orthologous genes, which show high frequency alterations in the TCGA dataset, are also indicated, with losses in blue and gains in red. The number within parenthesis indicates the percentage of samples bearing the given alteration in TCGA (single copy alterations). The asterisk indicates genes that are recurrently altered in mouse models. See also Figure S5, Tables S3–S6.

Table 1

Common Key Recurrent Genetic Alterations Between Human (TCGA) and Murine HGSCs

TCGA Cytoband	TCGA CNA (Wide Peak Start - End)	Mouse CNA[a]	Amp/Del	Gene	Pathway	Top 20 Significant TCGA Recurrent CNAs[b]
2q37.3	234758443 - 242951149	chr12:36,720,980-37,802,564[c]	Del			yes
4q23	89731957 - 117654338	chr3:127,451,904-141,625,646[c]	Del			yes
5q11.2	56048896 - 58137258	chr13:110,109,027-113,105,798[c]	Del			yes
5q13.1	66419415 - 74667916	chr13:95,262,550-104,324,218[c]	Del	*RAD17*	DNA Damage	yes
5q13.1	66419415 - 74667916	chr13:95,262,550-104,324,218[c]	Del	*PIK3R1*	PI3K/MYC	yes
5p13.2	21598644 - 45107526	chr15:3,114,799-181,356,650	Amp	*RICTOR*	PI3K/MYC	
5p13.2	21598644 - 45107526	chr15:3,114,799-181,356,650	Amp	*SKP2*	Cell Cycle/FOXM1	
6q21	92485304 - 127156139	chr10:29,810,651-58,578,139[c]	Del	*FOXO3*	PI3K/MYC	
8q24.3	144180457 - 146072839	chr15:75,090,979-78,428,406[c]	Amp	*MAPK15*	RAS/MAPK	yes
8q24.21	128754508 - 129388953	chr15:48,210,186-64,122,067	Amp	*MYC*[d]	PI3K/MYC	yes
11p15.5	1 - 4068254	chr7:108,811,066-150,762,912[c]	Del			yes
11q25	102218055 - 134452384	chr9:48,031,081-55,892,857[c]	Del	*ATM*	DNA Damage	
12p12.1	25059809 - 25394729	chr6:140,384,028-149,484,294[c]	Amp	*KRAS*[d]	RAS/MAPK	yes
12q24.33	74257132 - 132349534	chr10:82,071,334-111,202,977[c]	Del	*E2F7*	RB	
14q23.3	52629784 - 73351045	chr12:72,206,878-72,256,634[c]	Del	*NUMB*	NOTCH	
16q23.1	77190685 - 77350206	chr8:117,016,075-118,224,787	Del	*WWOX*	Tumor Suppressor Genes	
16q24.3	87965263 - 88055649	chr8:125,510,236-125,750,050	Del	*ANKRD11*	Tumor Suppressor Genes	
19p13.3	1 - 306931	chr10:77,929,170-80,249,143[c]	Del		Tumor Suppressor Genes	yes
19p13.3	1264798 - 4426322	chr10:77,929,170-80,249,143[c]	Del	*APC2*		yes
20q13.33	61411961 - 62435964	chr2:180,838,357-181,356,650[c]	Amp			yes

Recurrent changes occurring in 2 mouse models were found in cytobands *12p12.1*, *19.13.3*, and *2q37.3*; recurrent alterations occurring in 3 mouse models were found in cytobands *5q11.2* and *5q13.1*.

[a] Representative mouse CNA genomic coordinates are shown.

[b] Yes indicates included in the top 20 significant alterations.

[c] Denotes merged peak reported in TCGA.

[d] Gene is one of the top 20 significant genes in the TCGA dataset.

See also Figure S6.